Light-Assisted Oxidation of Single-Wall Carbon Nanohorns for Abundant Creation of Oxygenated Groups That Enable Chemical Modifications with Proteins To Enhance Biocompatibility

Minfang Zhang,[†,*] Masako Yudasaka,[†,‡,*] Kumiko Ajima,[†] Jin Miyawaki,[†] and Sumio Iijima[†,‡,§]

[†]SORST-JST, c/o NEC, 34 Miyukigaoka, Tsukuba, Ibaraki 305-8501, Japan, [‡]NEC, 34 Miyukigaoka, Tsukuba, Ibaraki 305-8501, Japan, and [§]Meijo University, 1-501 Shiogamaguchi, Tenpaku-ku, Nagoya 468-8502, Japan

ABSTRACT We show that light-assisted oxidation with hydrogen peroxide effectively and rapidly opens holes in carbon nanohorn walls and, more importantly, creates abundant oxygenated groups such as carboxylic groups at the hole edges. These oxygenated groups reacted with the protein bovine serum albumin. The obtained conjugates were highly dispersed in phosphate-buffered saline and were taken up by cultured mammalian cells *via* an endocytosis pathway.

KEYWORDS: carbon nanohorns · light-assisted oxidation · modification · dispersion · drug delivery

Carbon nanotubes[1,2] and nanohorns,[3] members of a class of nontoxic graphite, nanostructured carbon materials, are generating much enthusiasm in the field of drug delivery system (DDS) fabrication. Several reports of internalization of single-walled carbon nanotubes (SWNTs) by mammalian cells have appeared,[4–11] and effects of SWNT-DDS have been confirmed *in vitro*[9,10] and *in vivo*.[12,13] In addition to SWNTs, single-wall carbon nanohorns (SWNHs), which are single-graphene pseudotubules, have potential as DDSs.[14,15] Preliminary studies with SWNT-DDSs and SWNH-DDSs indicated some problems with the pharmacokinetics of SWNTs or SWNHs, particularly with respect to excretion of these compounds from living bodies.[16,17] Research so far has found that these compounds become trapped by the liver, lung, or spleen,[18,19] making it difficult to achieve complete excretion. One approach toward solving these problems was to increase the number of reactive sites on SWNTs and SWNHs through extensive chemical modification by biocompatible molecules.

The sites of chemical modification on carbon nanotubes are usually the groups containing oxygenated functionalities located at the cut ends or at defects in the sidewalls which have been created by oxidation. In studies on the oxidation of SWNTs, strong acids such as HNO_3, H_2SO_4, and H_2SO_4/H_2O_2 have usually been used.[20–23] However, it is difficult to control the extent of the reaction with these strong acids, resulting in the production of unwanted contaminants and even the induction of coalescence.[24,25] In contrast to strong acids, the use of H_2O_2, a milder oxidizing agent, is advantageous in controlling the degree of oxidation and for generating minimal amounts of carbonaceous byproduct.[26] In an earlier report, we observed that light irradiation during H_2O_2 oxidation effectively enhanced the oxidation rate while retaining the advantages of mild H_2O_2 oxidation conditions.[27] Light-assisted H_2O_2 oxidation (LAOx) seems to be the appropriate oxidation method; however, the generation of oxygenated groups has not been well characterized. Since the radicals $HOO^{\bullet}$ and $HO^{\bullet}$ are generated in LAOx,[28] we proposed that their reactions with SWNTs would create carboxylic acid (−COOH) groups. This is proved using SWNHs in this study. To verify the effect of LAOx, we chose to use SWNHs because they do not contain any metal catalysts and thus would minimize any artifacts caused by metal catalyst effects on the oxidation. We demonstrate in this report that the oxygenated groups created by LAOx are useful sites for chemical modifications. The LAOx-SWNHs were

*Address correspondence to minfang@frl.cl.nec.co.jp, yudasaka@frl.cl.nec.co.jp.

Received for review July 31, 2007 and accepted October 16, 2007.

Published online November 10, 2007.
10.1021/nn700130f CCC: $37.00

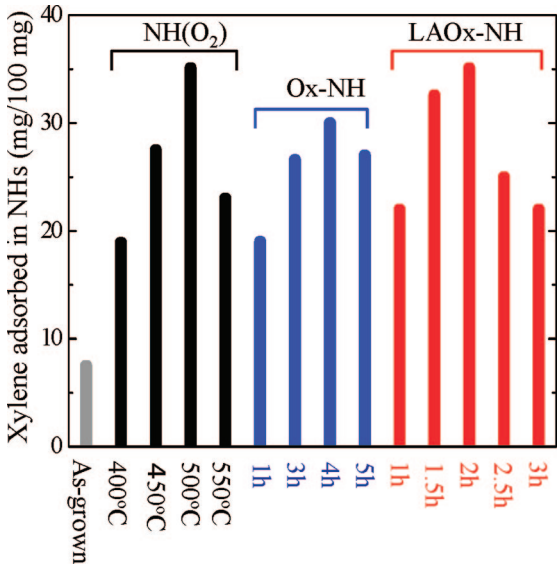

Figure 1. Effect of temperature and time of oxidation on xylene adsorption by SWNHs oxidized by different methods. Quantities of xylene adsorbed in as-grown SWNHs (gray), NH(O_2) for various T_{target} (black), Ox-NH with various t_{period} (blue), and LAOx-NH with various t_{period} (red) were estimated from differences in weight obtained during TGA.

modified with bovine serum albumin (BSA) through diimide-activated amidation, resulting in a product with enhanced hydrophilicity that readily dispersed in aqueous solution. We also observed that BSA-modified LAOx-SWNHs were incorporated into cultured mammalian cells *via* an endocytosis pathway.

RESULTS AND DISCUSSION

Opening Holes and Generating Carboxylic Acid Groups at the Hole Edges. To evaluate the extent of hole-opening in SWNHs as a result of oxidative processes, we previously quantitated the amount of nitrogen adsorption that occurred at 77 K,[29–32] or, alternatively, we estimated the quantity of xylene adsorption at room temperature.[33,34] We chose to use the latter method to estimate the degree of hole-opening of SWNHs because it gave results quickly while giving a good measurement of the pore volumes.[33] To show the efficiency of LAOx on the opening of holes in nanohorn structures, we compared SWNHs subjected to LAOx treatment for various periods of time (t_{period}-LAOx-NHs) with either (1) SWNHs treated with H_2O_2 for various periods of time but without light irradiation (t_{period}-Ox-NHs) or (2) SWNHs oxidized by heating in dry air over a temperature gradient ranging from room temperature to the target temperature (T_{target}) (NH(O_2,T_{target})).[33] The quantities of xylene adsorbed in as-grown SWNHs, LAOx-NHs, Ox-NHs, and NH(O_2) are shown in Figure 1, which were calculated from the thermogravimetric analysis (TGA) (Supporting Information). The maximum quantity of xylene adsorption occurred in the SWNHs after 2 h of LAOx treatment (2 h-LAOx-NHs). This degree of xylene adsorption exceeds the value for any of the t_{period}-Ox-NHs samples

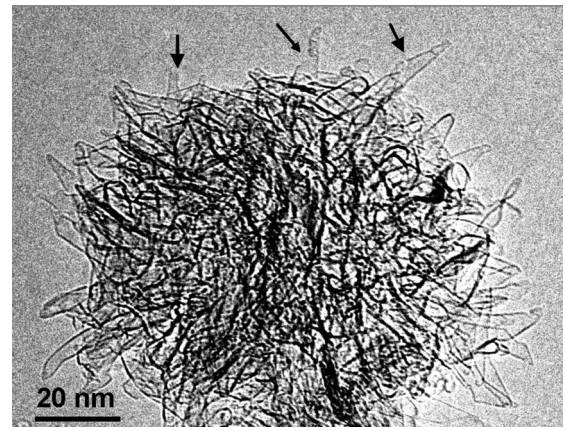

Figure 2. TEM image of 2 h-LAOx-NH. The arrows indicate the holes in the walls.

and was comparable with the largest value ever achieved by NH(O_2,T_{target}) (Figure 1 or ref 33). Furthermore, transmission electron microscopy (TEM) observations revealed holes in the walls of the 2 h-LAOx-NHs, with morphologies similar to those previously reported[35] (Figure 2). Oxygenated groups such as carboxylic acids, esters, ketones, aldehydes, and/or acid anhydrides were present in LAOx-NHs, as apparent from the broad peaks in the IR spectra (Figure 3) between 1600 and 1800 cm^{-1} which correspond to C═O stretching vibrations.[36–38] As the time of LAOx treatment in-

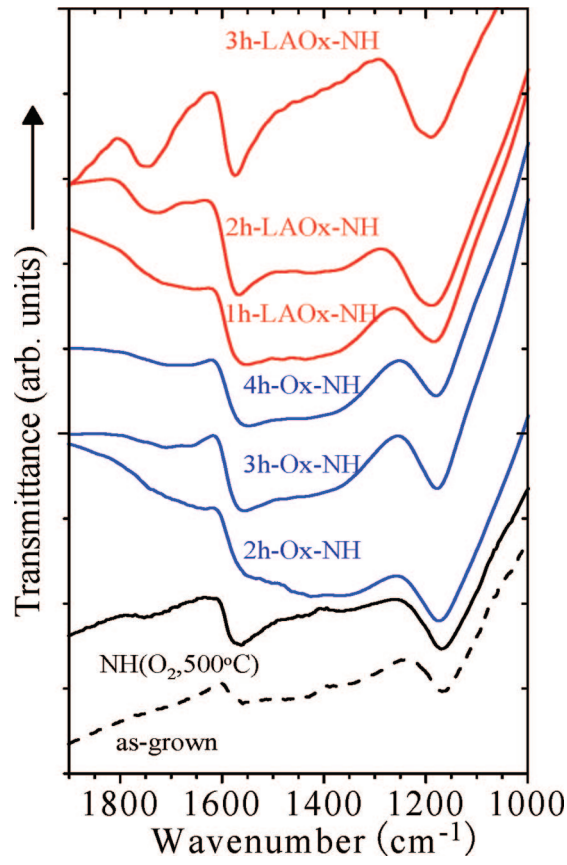

Figure 3. Infrared absorption spectra of as-grown SWNHs (black dashed), NH(O_2,500 °C) (black), Ox-NHs (blue), and LAOx-NHs (red).

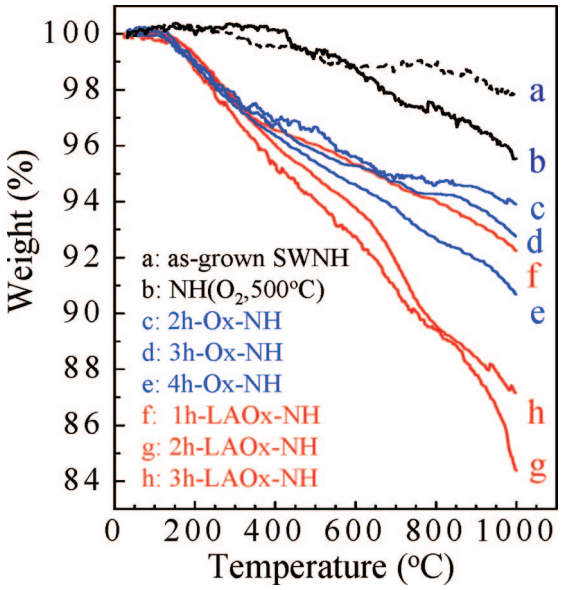

Figure 4. TGA results of as-grown SWNHs (black), NH(O_2,500 °C) (black), Ox-NHs (blue), and LAOx-NHs (red). The weight losses mainly correspond to the emission of CO_2 and/or CO, as revealed by the TPD measurements shown in Figure 5.

creased, the peak maximum was more blue-shifted. Short-term LAOx tended to create ketones and aldehydes, while the longer term LAOx tended to produce carboxylic and acid anhydride species. The number of oxygenated groups in NH(O_2,500 °C) was small, and the number in the as-grown SWNHs was even smaller. Two broad peaks at ~1170 and ~1560 cm^{-1} in the spectrum of as-grown SWNHs are associated with, respectively, the C—O stretching of saturated aliphatic ethers and the stretching of aromatic rings or C═C that were conjugated with C═O groups existing nearby.[38] These two peaks were also blue-shifted after the oxidations, possibly indicating the advent of C—O of esters and an increase in C═O numbers, respectively. Notably, the peaks relevant to the oxygenated groups increased in intensity as the time of the oxidation period increased, with this tendency being most remarkable in the LAOx-NHs.

TGA showed that the weight losses of 2 h-LAOx-NHs and 3 h-LAOx-NHs due to the decomposition of oxygenated groups exceeded those of the 1 h-LAOx-NHs and Ox-NHs and were much larger than those of NH(O_2,500 °C) and as-grown SWNHs (Figure 4). The temperature-programmed desorption mass spectroscopy (TPD-MS) spectra (Figure 5) indicated that CO_2 was emitted from the 2 h-LAOx-NHs over a wide temperature range between 200 and 1000 °C, with two maxima at 230 and 700 °C. The former reflected the decomposition of the carboxylic acid groups, and the latter reflected the decomposition of lactone or carboxylic acid anhydrides groups.[39] The 3 h-LAOx-NHs had the highest peak, at 700 °C, so it was rich in lactone groups and carboxylic acid anhydrides. The nanohorns oxidized with only H_2O_2 without light irradiation, and the 1 h-

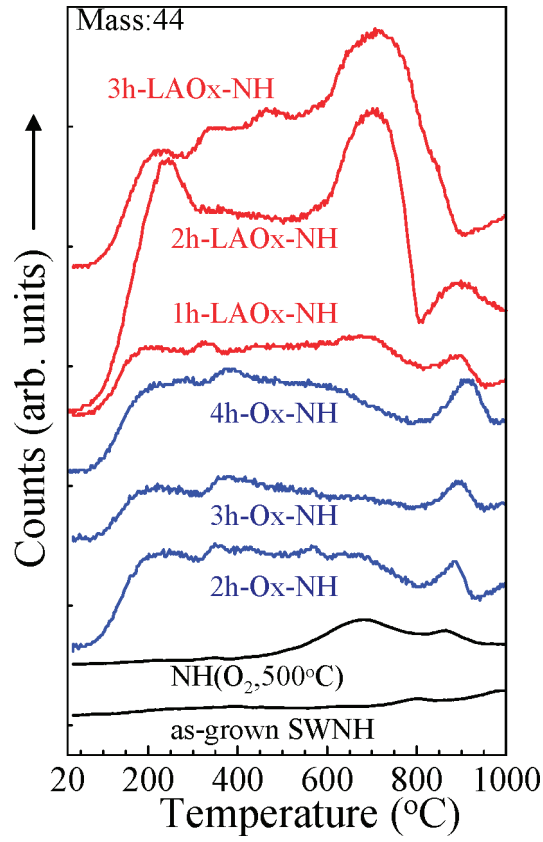

Figure 5. CO_2 emission measured by TPD-MS. As-grown SWNHs (black), NH(O_2,500 °C) (black), Ox-NHs (blue), and LAOx-NHs (red).

LAOx-NHs had fewer oxygenated groups. Unlike the H_2O_2-oxidized LAOx-NHs and Ox-NHs, the O_2-oxidized NH(O_2,500 °C) had peaks at temperatures higher than 500 °C, indicating that it was poor in carboxylic acid groups. All samples displayed emission at temperatures above 1000 °C (not shown), which corresponded to CO and suggested the presence of carbonyl, phenol, or quinone groups.[39]

From the TPD data (Figure 5), it is reasonable to consider that carboxylic groups combusted below 500 °C; therefore, we estimated the number of carboxylic acid groups in 2 h-LAOx-NH from the weight loss below 500 °C in TGA (Figure 4). The weight decrease in this range was about 6%, wherefrom we estimated that there were about 350 carboxylic groups in one nanohorn. This number of carboxylic groups seems too high as compared with the TEM image in Figure 2. Some carboxylic groups located at the edges of small holes may not have been visible with TEM.

Hydrogen peroxide is known to generate the highly reactive radicals $HOO^{\bullet}$ and $HO^{\bullet}$ when irradiated by light with a wavelength of 250–400 nm.[28] Such radicals may attack the defects at the sidewalls or tips of SWNHs and form oxygenated groups. We propose that these oxygenated groups are rapidly and sequentially degraded by the $HOO^{\bullet}$ and $HO^{\bullet}$ radicals, so holes are quickly opened and their diameters become larger.

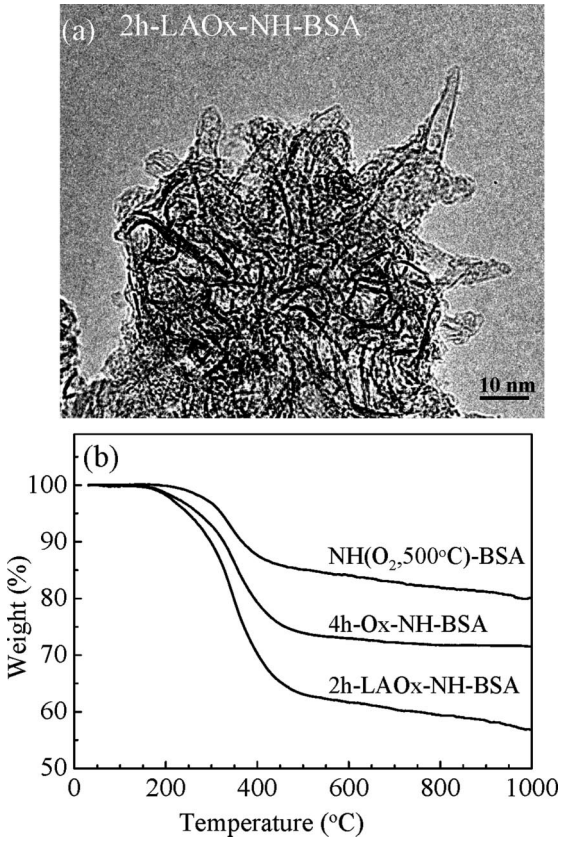

Figure 6. (a) TEM image of 2 h-LAOx-NH−BSA. (b) TGA results of 2 h-LAOx-NH−BSA, 4 h-Ox-NH−BSA, and NH(O_2,500 °C)−BSA.

When SWNHs are treated with H_2O_2 without light irradiation, a reaction may occur between the SWNHs and the anions $^-$OOH and $^-$OH.[28] Since these anions will be less reactive than the radicals, the reaction rate in the absence of light should be slower, although the oxygenated groups are still likely to be rich in the carboxylic acids. In the case of oxidation with O_2 at a high temperature, such as 500 °C, holes can be effectively opened in the walls of SWNHs,[33] but the high oxidation temperature induces the creation of ketone- or quinone-related groups rather than carboxylic-related groups.

Chemical Modification of LAOx SWNHs with a Protein, BSA. To demonstrate that the oxygenated groups are useful sites for the chemical modification of SWNHs, BSA was reacted with 2 h-LAOx-NHs, 4 h-Ox-NHs, and NH(O_2,500 °C) *via* diimide-activated amidation according to the procedures applied to SWNTs.[40] The obtained conjugates are referred to as 2 h-LAOx-NH−BSA, 4 h-Ox-NHs−BSA, and NH(O_2,500 °C)−BSA, respectively.

TEM images of 2 h-LAOx-NH−BSA showed the presence of molecules attached to the outer surface of SWNHs (Figure 6a), which were not visible in 2 h-LAOx-NH (Figure 2). They were probably BSA molecules, possibly damaged to various extents by electron beams during the acquisition of TEM data. BSA

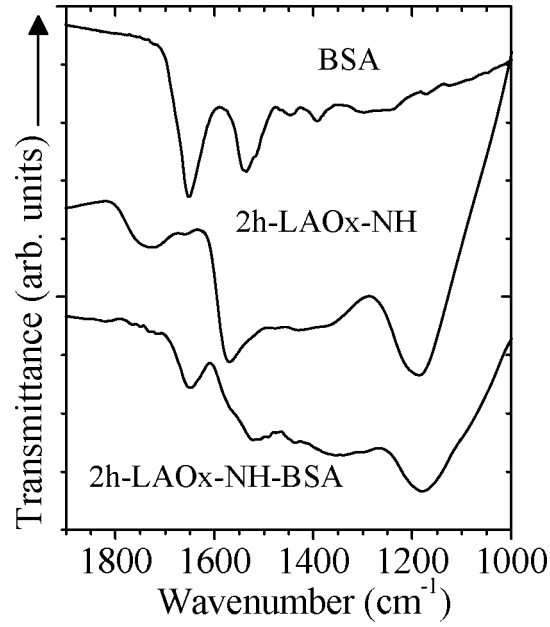

Figure 7. FT-IR spectra of 2 h-LAOx-NH−BSA, 2 h-LAOx-NH, and BSA.

molecules are known to take various forms, depending on the atmosphere or surrounding/contacting materials.[41] The molecules may be 3 nm thick and 8 nm wide in a compact form, 4 nm wide and 13 nm long for the folded type, or 2 nm wide and 25 nm long in the extended form. In these TEM images (Figure 6a), the BSA molecules appear to have taken the extended form rather than compact or folded forms, and they have wrapped around the surface of the SWNH. Since BSA contains hydrophobic and hydrophilic residues, we conjecture that the hydrophobic groups made contact with the graphene wall of the SWNH.

The quantities of BSA attached to SWNHs were estimated by TGA as the weight-loss differences before (Figure 4) and after (Figure 6b) BSA attachment. These quantities were 27% for 2 h-LAOx-NH−BSA (0.37 g/g in weight ratio of BSA to 2 h-LAOx-NH), which was larger than either 20% (0.25 g/g) for 4 h-Ox-NH−BSA or 16% (0.19 g/g) for NH(O_2,500 °C)−BSA. These indicated that the individual SWNH had one or two BSA molecules attached, which agrees reasonably well with the TEM image in Figure 6a. In the above calculations, one SWNH tubule with a diameter of 2−4 nm and length of 40−50 nm^3 was assumed to have ~20 000 carbon atoms. The BSA molecular weight was 66 000.

The formation of covalent bonds between 2 h-LAOx-NH and BSA was confirmed by IR spectroscopy. In comparison to the 2 h-LAOx-NH spectrum, the intensities of the absorption bands related to C═O and/or C—O of the oxygenated groups decreased remarkably in the 2 h-LAOx-NH−BSA samples, and new absorption bands appeared at 1650 and 1525 cm^{-1} (Figure 7). These two new peaks corresponded to C═O stretching (1650 cm^{-1}) and N—H bending (1540 cm^{-1}) of

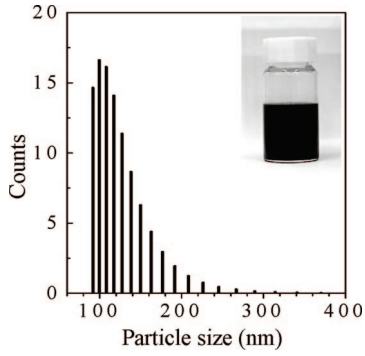

Figure 8. Particle-size distribution of 2 h-LAOx-NH−BSA dispersed in PBS, measured by the dynamic light scattering method. The inset photograph indicates the dispersion of 2 h-LAOx-NH−BSA in PBS.

amide linkages.[36] Therefore, it is apparent that the oxygenated groups of 2 h-LAOx-NH were involved in the reaction with BSA. The peak for 2 h-LAOx-NH at 1170–1190 cm^{-1} remained even after the reaction with BSA, which supports the above-mentioned assignment of this peak to the C—O stretching of the saturated aliphatic ether groups.

According to the study by Huang *et al.*,[40] BSA attachment should enhance the dispersion of SWNHs in aqueous solutions. We prepared a homogeneous dispersion of 2 h-LAOx-NH−BSA in phosphate-buffered saline (PBS) (Figure 8, inset) and documented that it was very stable for several weeks, while the dispersions of Ox-NH−BSA and NH(O_2,500 °C)−BSA (pictures not shown) survived for only a few days. This result implies that the larger amount of covalently linked BSA responded to the higher dispersion of SWNHs in aqueous solutions. When we examined the dispersion of 2 h-LAOx-NH−BSA in PBS using the dynamic light scattering method, we found that the particle sizes distributed around 90–140 nm (Figure 8). These values are a little higher than those for the bare SWNH aggregates (80–100 nm[3]), indicating that 2 h-LAOx-NH−BSA was dispersed almost individually in PBS. The slightly larger size was caused by BSA unfolding from 2 h-LAOx-NH.

Cellular Uptake of SWNH−BSA Conjugates. We attached BSA covalently modified with the dye Alexa Fluor 488 (BSA-AF) to 2 h-LAOx-NH (2 h-LAOx-NH−BSA-AF) and dispersed the sample into PBS. Laser confocal microscopy showed that SWNHs aggregates agglomerated and appeared as dark or pale spots in the differential interference contrast (DIC) image (Figure 9b). All of the aggregates appeared as green spots in the fluorescence images (Figure 9a,c), reflecting that 2 h-LAOx-NH reacted well with BSA-AF.

When H460 cancer cells were incubated with the dispersion of 2 h-LAOx-NH−BSA-AF for 2 h at 37 °C, cellular uptake was observed with the confocal microscope. The fluorescent image (Figure 10a), the DIC image (Fig-

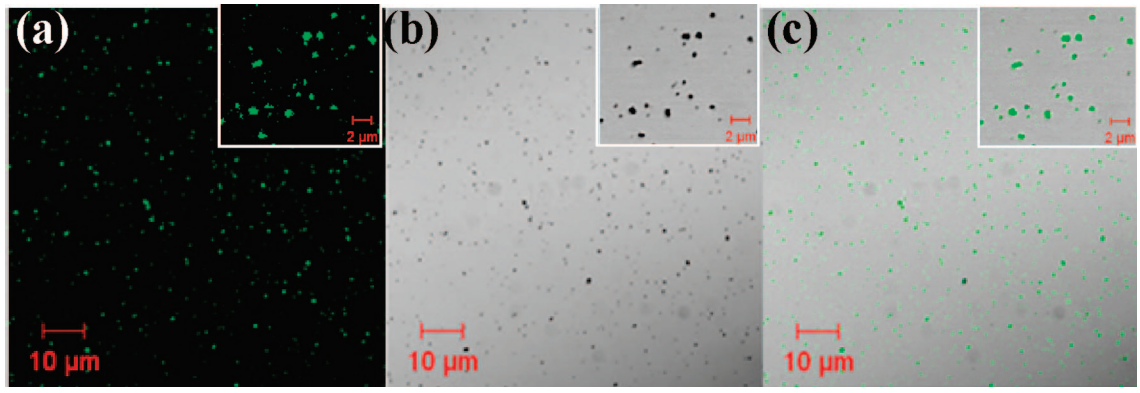

Figure 9. Confocal microscope images (excitation λ = 488 nm, emission detected at λ = 510 nm) of 2 h-LAOx-NH−BSA-AF. Fluorescence (a), DIC (b), and a combination of fluorescence and DIC images (c).

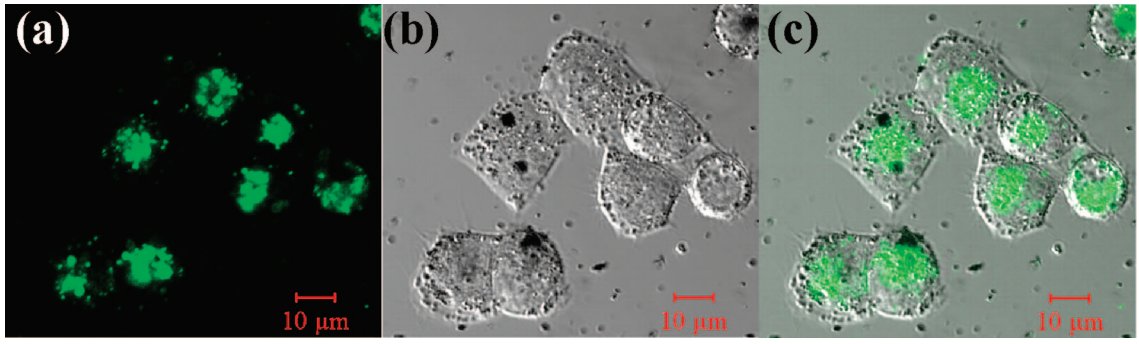

Figure 10. Confocal microscope images of H460 cells after incubation with 2 h-LAOx-NH−BSA-AF in PBS for about 2 h. Fluorescence (a), DIC (b), and a combination of fluorescence and DIC images (c).

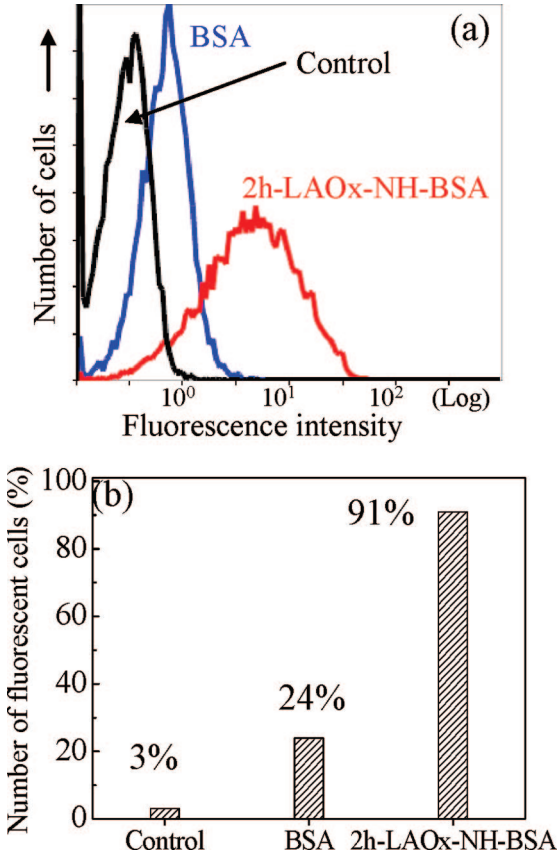

Figure 11. Flow cytometry data of the H460 cells (excitation, 488 nm; detection, 525 nm): (a) control (black), incubated with BSA-AF (blue), and incubated with 2 h-LAOx-NH−BSA-AF (red). (b) The percentage of cells with fluorescence.

ure 10b), and their combination (Figure 10c) revealed that the fluorescence was mainly emitted from the cell interior, indicating that the 2 h-LAOx-NH−BSA-AF was taken inside the cells. We also note that the fluorescent particles in Figure 10a were much larger than those in Figure 9a, suggesting that 2 h-LAOx-NH−BSA-AF particles agglomerated inside the cells. The flow cytometry measurements revealed that about 91% of the H460 cells took 2 h-LAOx-NH−BSA-AF into the interiors (Figure 11).

For reference, we incubated H460 cells with BSA-AF instead of the 2 h-LAOx-NH−BSA-AF complex and similarly analyzed the cellular uptake. The flow cytometry results showed only about 24% cellular uptake (Figure 11). Thus, the uptake of BSA-AF by the H460 cells was not a frequent event, and the majority of the green spots in Figure 10 cannot be attributed to unreacted BSA-AF.

To study the mechanism of the cellular uptake of 2 h-LAOx-NH−BSA, we incubated the cells with PBS containing 2 h-LAOx-NH−BSA-AF at 4 °C for about 2 h. The confocal microscope images (Figure 12) revealed that the 2 h-LAOx-NH−BSA-AF was located mainly around the cell membranes but not inside the cells, indicating that the cell internalization was energy dependent. Thus, endocytosis[42] is a possible cellular uptake pathway for these nanostructures.

CONCLUSIONS

We found that light-assisted oxidation with H_2O_2 (LAOx), was effective in creating abundant oxygenated groups, such as carboxylic acid groups, at hole edges as well as causing the rapid opening of holes in the graphene walls of SWNHs. BSA was attached to the oxygenated groups *via* diimide-activated amidation. More BSA molecules were attached to the 2 h-LAOx-NH−BSA than to either 4 h-Ox-NH−BSA or NHox(O_2,500 °C)−BSA, indicating the superiority of LAOx for generating sites for covalent linkages. The abundant attachment of BSA caused 2 h-LAOx-NH−BSA to disperse in PBS almost as individual particles, and homogeneous dispersion was maintained for a long period. This fine dispersion enabled the internalization of 2 h-LAOx-NH−BSA inside mammalian cells. The uptake mechanism was considered to be endocytosis because it was suppressed at 4 °C.

We think that LAOx should be effective on other carbon forms, such as nanotubes. This oxidation technique should increase the potential for chemical modification of nanostructures and should broaden their various applications.

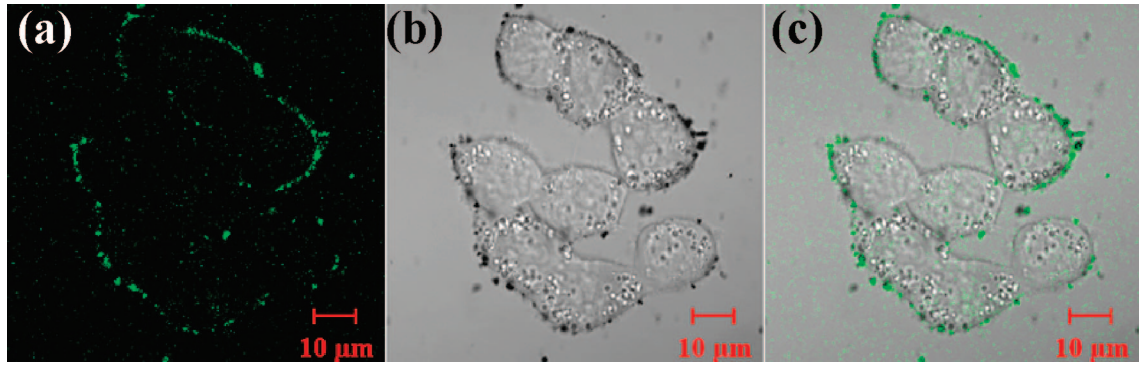

Figure 12. Confocal microscope images of H460 cells after incubation with 2 h-LAOx-NH−BSA-AF for 2 h at 4 °C. Fluorescence (a), DIC (b), and a combination of fluorescence and DIC images (c).

MATERIALS AND EXPERIMENTS

Opening Holes and Generating Oxygenated Groups at the Hole Edges. The SWNHs were generated by laser vaporization of pure graphite;[3] the purity was about 95%.[43] The LAOx method was similar to that previously used for SWNTs.[27,44] Briefly, a dispersion of about 40 mg of as-grown SWNHs in 50 mL of 30% H_2O_2 aqueous solution was stirred on a hot plate set at 100 °C and irradiated with a Xe lamp (wavelength, 250–2000 nm; intensity; 3 W; diameter, 1 cm). After LAOx for various periods of time (t_{period} = 1–5 h), the SWNH suspension was immediately filtered and washed 3–5 times with deionized water. The obtained t_{period}-LAOx-NHs were lyophilized for about 48 h. For reference, SWNHs treated with H_2O_2 without light irradiation (t_{period}-Ox-NHs) and SWNHs oxidized in dry air by heating from room temperature to a target temperature (T_{target}) at an temperature elevation rate of 1 °C/min followed by natural cooling, termed (NH(O_2,T_{target})),[33] were also prepared.

To confirm that holes were opened by LAOx, we quantitated the xylene adsorption by previously established methods.[33,34] Briefly, the SWNHs after hole-opening were exposed to xylene vapor for 1 h in a closed container. Using thermogravimetric analysis (TGA) performed in helium, the quantities of adsorbed xylene were estimated from the weight loss occurring below 300 °C.

IR spectra of the SWNHs samples were measured in the spectrum region of 400–4000 cm^{-1} by using a Perkin-Elmer FT-IR spectrophotometer. TGA and TPD-MS measurements, used for quantifying the oxygenated groups in SWNHs, were performed from room temperature to 1000 °C in helium with a heating rate of 10 °C/min.

Chemical Modification of LAOx SWNHs with BSA. The chemical modification of 2 h-LAOx-NHs with BSA followed the previously published procedures applied to SWNTs.[40] We dispersed ~35 mg of 2 h-LAOx-NHs in a 50-mL phosphate buffer solution, pH 7.4, using a bath-type sonicator for 30 min. 1-Ethyl-3-[3-(dimethylamino)propyl]carbodiimide (EDAC) (140 mg) was added, and the mixture was stirred for about 2 h. Bovine serum albumin (BSA, Sigma-Aldrich, 66 kDa, ~350 mg) was added to the dispersion of SWNHs and further stirred at room temperature for about 24 h. Nonreacted EDAC and BSA were removed by washing with deionized water through repeated filtration and dispersion. The washing was repeated until the filtrate became free of BSA, which was confirmed by the absence of the BSA absorption band in the ultraviolet–visible–near-infrared (UV–vis–NIR) spectrum. After the washing, 2 h-LAOx-NH–BSA was dried at 70 °C for 48 h in air. For reference, 4 h-Ox-NHs and NH(O_2,500 °C) were similarly modified with BSA to obtain 4 h-Ox-NHs–BSA and NH(O_2,500 °C)–BSA, respectively.

For the cellular uptake experiments, 2 h-LAOx-NH was also modified with Alexa Fluor 488-labeled BSA (BSA-AF, purchased from Molecular Probes). The as-washed 2 h-LAOx-NH–BSA-AF without further drying was dispersed in PBS, and the concentration was diluted to 0.002 mg/mL.

Cellular Uptake of SWNH–BSA Conjugates. Human lung cancer cells H460 (purchased from ATCC) were seeded in 35-mm dishes and grown in RPMI 1640 cell culture medium supplemented with 10% fetal bovine serum and 0.1% penicillin–streptomycin. The cell density in the medium solution was ~2×10^4 cells/mL. After incubation for 24 h at 37 °C in 5% CO_2 atmosphere, we replaced the cell culture medium with the dispersion of 2 h-LAOx-NH–BSA-AF in PBS (0.002 mg/mL) and incubated the culture for about 2 h at 37 or 4 °C. We then removed the 2 h-LAOx-NH–BSA-AF dispersion and washed the cells with fresh culture medium solution. The cellular uptake of 2 h-LAOx-NH–BSA-AF was investigated with a confocal microscope (LSM5 Pascal, Zeiss) and a flow cytometer (Beckman, Cytomics FC500). For the flow cytometry measurements, the cultured cells were detached from the dish bottoms using 0.25% trypsin–EDTA and dispersed in the fresh culture medium. The excitation wavelength was 488 nm, and the fluorescence emission was detected at 525 nm.

Acknowledgment. We thank Dr. T. Azami and Dr. D. Kasuya of NEC Corporation for supporting the SWNH preparation.

Supporting Information Available: Thermogravimetric analysis results of as-grown SWNHs, LAOx-NHs, and Ox-NHs after xylene adsoption for 1 h. This material is available free of charge *via* the Internet at http://pubs.acs.org.

REFERENCES AND NOTES

1. Iijima, S. Helical Microtubules of Graphitic Carbon. *Nature* **1991**, *354*, 56–58.
2. Iijima, S.; Ichihashi, T. Single-Shell Carbon Nanotubes of 1-nm Diameter. *Nature* **1993**, *363*, 603–605.
3. Iijima, S.; Yudasaka, M.; Yamada, R.; Bandow, S.; Suenaga, K.; Kokai, F.; Takahashi, K. Nano-Aggregates of Single-Walled Graphitic Carbon Nano-Horns. *Chem. Phys. Lett.* **1999**, *309*, 165–170.
4. Kam, N. W. S.; Jessop, T. C.; Wender, P. A.; Dai, H. Nanotube Molecular Transporters: Internalization of Carbon Nanotube–Protein Conjugates into Mammalian Cells. *J. Am. Chem. Soc.* **2004**, *126*, 6850–6851.
5. Lu, Q.; Moore, J. M.; Huang, G.; Mount, A. S.; Rao, A. M.; Larcom, L. L.; Ke, P. C. RNA Polymer Translocation with Single-Walled Carbon Nanotubes. *Nano Lett.* **2004**, *4*, 2473–2477.
6. Pantarotto, D.; Briand, J.; Prato, M.; Bianco, A. Translocation of Bioactive Peptides across Cell Membranes by Carbon Nanotubes. *Chem. Commun.* **2004**, *1*, 16–17.
7. Cherukuri, P.; Bachilo, S. M.; Litovsky, S. H.; Weisman, R. B. Near-Infrared Fluorescence Microscopy of Single-Walled Carbon Nanotubes in Phagocytic Cells. *J. Am. Chem. Soc.* **2004**, *126*, 15638–15639.
8. Bianco, A.; Kostarelos, K.; Partidos, C. D.; Prato, M. Biomedical Application of Functionalised Carbon Nanotubes. *Chem. Commun.* **2005**, *5*, 571–577.
9. Kam, N. W. S.; Dai, H. Carbon Nanotubes as Intracellular Protein Transporters: Generality and Biological Functionality. *J. Am. Chem. Soc.* **2005**, *127*, 6021–6026.
10. Kam, N. W. S.; O'Connell, M.; Wisdom, J. A.; Dai, H. Carbon Nanotubes as Multifunctional Biological Transporters and Near-Infrared Agents for Selective Cancer Cell Destruction. *Proc. Natl. Acad. Sci. U.S.A.* **2005**, *102*, 11600–11605.
11. Isobe, H.; Tanaka, T.; Maeda, R.; Noiri, E.; Solin, N.; Yudasaka, M.; Iijima, S.; Nakamura, E. Preparation, Purification, Characterization, and Cytotoxicity Assessment of Water-Soluble, Transition-Metal-Free Carbon Nanotube Aggregates. *Angew. Chem., Int. Ed.* **2006**, *45*, 6676–6680.
12. Liu, Z.; Cai, W.; He, L.; Nakayama, N.; Chen, K.; Sun, X.; Chen, X.; Dai, H. *In vivo* Biodistribution and Highly Efficient Tumour Targeting of Carbon Nanotubes in Mice. *Nat. Nanotechnol.* **2006**, *2*, 47–52.
13. Yang, R.; Yang, X.; Zhang, Z.; Zhang, Y.; Wang, S.; Cai, Z.; Jia, Y.; Ma, Y.; Zheng, C.; Roden, R.; Chen, Y. Single-Walled Carbon Nanotubes-Mediated *in vivo* and *in vitro* Delivery of siRNA into Antigen-presenting Cells. *Gene Ther.* **2006**, *13*, 1714–1723.
14. Murakami, T.; Ajima, K.; Miyawaki, J.; Yudasaka, M.; Iijima, S.; Shiba, K. Drug-Loaded Carbon Nanohorns: Adsorption and Release of Dexamethasone in Vitro. *Mol. Pharm.* **2004**, *1*, 399–405.
15. Ajima, K.; Yudasaka, M.; Murakami, T.; Maigne, A.; Shiba, K.; Iijima, S. Carbon Nanohorns as Anticancer Drug Carriers. *Mol. Pharm.* **2005**, *2*, 475–480.
16. Cherukuri, P.; Gannon, C.; Leeuw, T.; Schmidt, H. K.; Smalley, R.; Curley, S.; Weisman, R. Mammalian Pharmacokinetics of Carbon Nanotubes Using Intrinsic Near-Infrared Fluorescence. *Proc. Natl. Acad. Sci. U.S.A.* **2006**, *103*, 18882–18886.
17. Singh, R.; Pantarotto, D.; Lacerda, L.; Pastorin, G.; Klumpp, C.; Prato, M.; Bianco, A.; Kostarelos, K. Tissue Biodistribution and Blood Clearance Rates of Intravenously Administered Carbon Nanotube Radiotracers. *Proc. Natl. Acad. Sci. U.S.A.* **2006**, *103*, 3357–3362.
18. Wang, H.; Wang, J.; Deng, X.; Sun, H.; Shi, Z.; Gu, Z.; Liu, Y.; Zhao, Y. Preparation and Biodistribution of 125I-Labeled Water-Soluble Single-Wall Carbon Nanotubes. *J. Nanosci. Nanotechnol.* **2004**, *4*, 8.

19. Yang, S.; Guo, W.; Lin, Y.; Deng, X.; Wang, H.; Sun, H.; Liu, Y.; Wang, X.; Wang, W.; Chen, M.; *et al.* Biodistribution of Pristine Single-Walled Carbon Nanotubes. *J. Phys. Chem. C* **2007**, published online June 19, http://dx.doi.org/10.1021/jp070712c.
20. Tsang, S.; Chen, Y.; Harris, P.; Green, M. A Simple Chemical Method of Opening and Filling Carbon Nanotubes. *Nature* **1994**, *372*, 159–162.
21. Hiura, H.; Ebbesen, T.; Tanigaki, K. Opening and Purification of Carbon Nanotubes in High Yields. *Adv. Mater.* **1995**, *7*, 275–276.
22. Liu, J.; Rinzler, A.; Dai, H.; Hafner, J.; Bradley, R.; Boul, P.; Lu, A.; Iverson, T.; Shelimov, K.; Huffman, C.; *et al.* Fullerene Pipes. *Science* **1998**, *280*, 1253–1256.
23. Che, J.; Hammon, M. A.; Hu, H; Chen, Y, S.; Rao, A. M.; Eklund, P. C.; Haddon, R. C. Solution Properties of Single-Walled Carbon Nanotubes. *Science* **1998**, *282*, 95–98.
24. Zhang, M.; Yudasaka, M.; Iijima, S. Diameter Enlargement of Single-Wall Carbon Nanotubes by Oxidation. *J. Phys. Chem. B* **2004**, *108*, 149–153.
25. Yang, C.; Kasuya, D.; Yudasaka, M.; Iijima, S.; Kaneko, K. Microporosity Development of Single-Wall Carbon Nanohorn with Chemically Induced Coalescence of the Assembly Structure. *J. Phys. Chem. B* **2004**, *108*, 17775–17782.
26. Kataura, H.; Maniwa, Y.; Abe, M.; Fujiwara, A.; Kodama, T.; Kikuchi, K.; Imahori, H.; Misaki, Y.; Suzuki, S.; Achiba, Y. Optical Properties of Fullerene and Non-Fullerene Peapods. *Appl. Phys. A: Mater. Sci. Process.* **2002**, *74*, 349–354.
27. Yudasaka, M.; Zhang, M.; Iijima, S. Diameter-Selective Removal of Single-Wall Carbon Nanotubes through Light-Assisted Oxidation. *Chem. Phys. Lett.* **2003**, *374*, 132–136.
28. Schumb, W.,*et al. Hydrogen Peroxide*; Reinhold: New York, 1955.
29. Murata, K.; Kaneko, K.; Steele, W. A.; Kokai, F.; Takahashi, K.; Kasuya, D.; Yudasaka, M.; Iijima, S. Porosity Evaluation of Intrinsic Intraparticle Nanopores of Single Wall Carbon Nanohorn. *Nano Lett.* **2001**, *1*, 197–199.
30. Bekyaroya, E.; Kaneko, K.; Kasuya, D.; Murada, K.; Yudasaka, M.; Iijima, S. Oxidation and Porosity Evaluation of Budlike Single-Wall Carbon Nanohorn Aggregates. *Langmuir* **2002**, *18*, 4138–4141.
31. Murata, K.; Kaneko, K.; Kanoh, H.; Kasuya, D.; Takahashi, K.; Kokai, F.; Yudasaka, M.; Iijima, S. Adsorption Mechanism of Supercritical Hydrogen in Internal and Interstitial Nanospaces of Single-Wall Carbon Nanohorn Assembly. *J. Phys. Chem. B* **2002**, *106*, 11132–11138.
32. Utsumi, S.; Miyawaki, J.; Tanaka, H.; Hattori, Y.; Itoi, T.; Ichikuni, N.; Kanoh, H.; Yudasaka, M.; Iijima, S.; Kaneko, K. Opening Mechanism of Internal Nanoporosity of Single-Wall Carbon Nanohorn. *J. Phys. Chem. B* **2005**, *109*, 14319–14324.
33. Fan, J.; Yudasaka, M.; Miyawaki, J.; Ajima, K.; Murata, K.; Iijima, S. Control of Hole Opening in Single-Wall Carbon Nanotubes and Single-Wall Carbon Nanohorns Using Oxygen. *J. Phys. Chem. B* **2006**, *110*, 1587–1591.
34. Yudasaka, M.; Fan, J.; Miyawaki, J.; Iijima, S. Studies on the Adsorption of Organic Materials Inside Thick Carbon Nanotubes. *J. Phys. Chem. B* **2005**, *109*, 8909–8913.
35. Ajima, K.; Yudasaka, M.; Suenaga, K.; Kasuya, D.; Azami, T.; Iijima, S. Material Storage Mechanism in Porous Nanocarbon. *Adv. Mater.* **2004**, *16*, 397–401.
36. Socrates, G. *Infrared Characteristic Group Frequencies*; Wiley: New York, 1980.
37. Moreno-Castilia, C.; Carrasco-Marin, F.; Maldonado-Hodar, F. J.; Rivera-Utailia, J. Effects of Non-Oxidant and Oxidant Acid Treatment on the Surface Properties of An Activated Carbon with Very Low Ash Content. *Carbon* **1998**, *36*, 145–151.
38. Mawhinney, D. B.; Naumenko, V.; Kuznetsova, A.; Yates, J. T., Jr.; Liu, J.; Smalley, R. E. Infrared Spectral Evidence for the Etching of Carbon nanotubes: Ozone Oxidation at 298 K. *J. Am. Chem. Soc.* **2000**, *122*, 2383–2384.
39. Figueiredo, J. L.; Pereira, M. F. R.; Freitas, M. M. A.; Orfao, J. J. M. Modification of the Surface Chemistry of Activated Carbons. *Carbon* **1999**, *37*, 1379–1389.
40. Huang, W.; Taylor, S.; Fu, K.; Lin, Y.; Zhang, D.; Hanks, T.; Rao, A.; Sun, Y. Attaching Proteins to Carbon Nanotubes via Diimide-Activated Amidation. *Nano Lett.* **2002**, *2*, 311–314.
41. Das, A.; Chitra, R.; Choudhury, R. R.; Ramanadham, M. Structural Changes During the Unfolding of Bovine Serum Albumin in the Presence of Urea: A Small-Angle Neutron Scattering Study. *Pramana J. Phys.* **2004**, *63*, 363–368.
42. Silverstein, S. C.; Steinman, R. M.; Cohn, Z. A. Endocytosis. *Annu. Rev. Biochem.* **1977**, *46*, 669–722.
43. Azami, T.; Kasuya, D.; Yoshitake, T.; Kubo, Y.; Yudasaka, M.; Iijima, S. Large Scale Production of Carbon Nanohorns with High Purity. *The 30th Fullerene-Nanotubes General Symposium*, Japan, 2006; p 172.
44. Zhang, M.; Yudasaka, M.; Miyauchi, Y.; Maruyama, S.; Iijima, S. Changes in the Fluorescence Spectrum of Individual Single-Wall Carbon Nanotubes Induced by Light-Assisted Oxidation with Hydroperoxide. *J. Phys. Chem. B* **2006**, *110*, 8935–8940.